Aalto University

OPEN ACCESS

This is an electronic reprint of the original article.
This reprint may differ from the original in pagination and typographic detail.

Monticeli, Francisco; Almeida, Humberto; Neves, Roberta; Ornaghi, Felipe; Ornaghi Jr, Heitor L

On the 3D void formation of hybrid carbon/glass fiber composite laminates: A statistical approach

Published in:
Composites Part A : Applied science and manufacturing

DOI:
10.1016/j.compositesa.2020.106036

Published: 01/10/2020

Document Version
Peer-reviewed accepted author manuscript, also known as Final accepted manuscript or Post-print

Published under the following license:
CC BY-NC-ND

Please cite the original version:
Monticeli, F., Almeida, H., Neves, R., Ornaghi, F., & Ornaghi Jr, H. L. (2020). On the 3D void formation of hybrid carbon/glass fiber composite laminates: A statistical approach. *Composites Part A : Applied science and manufacturing*, *137*, 1-10. Article 106036. https://doi.org/10.1016/j.compositesa.2020.106036

This material is protected by copyright and other intellectual property rights, and duplication or sale of all or part of any of the repository collections is not permitted, except that material may be duplicated by you for your research use or educational purposes in electronic or print form. You must obtain permission for any other use. Electronic or print copies may not be offered, whether for sale or otherwise to anyone who is not an authorised user.

On the 3D void formation of hybrid carbon/glass fiber composite laminates: a statistical approach

Francisco M. Monticeli[a]*, José Humberto S. Almeida Jr[b], Roberta M. Neves[c], Felipe G. Ornaghi[d], Heitor L. Ornaghi Jr.[e]

[a]*Department of Materials and Technology, São Paulo State University, Guaratinguetá, SP, Brazil;* *francisco_monticelli@hotmail.com*

[b]*Department of Mechanical Engineering, Aalto University, Espoo, Finland;* *humberto.almeida@aalto.fi*

[c]*PPGE3M, Federal University of Rio Grande do Sul, Porto Alegre, RS, Brazil;* *robertamneves@gmail.com*

[d]*PGCIMAT, Federal University of Rio Grande do Sul, Porto Alegre, RS, Brazil;* *fgornagh@gmail.com*

[e] PGMAT, *Caxias do Sul University*, Caxias do Sul, RS, Brazil; *ornaghijr.heitor@gmail.com*

*Corresponding author. E-mail address: francisco_monticelli@hotmail.com

---

Abstract

The main objective of this study is to analyze the effect of the stacking sequence of hybrid laminates on the 3D void formation via a statistical approach. For that purpose, a three-dimensional microstructure is created from planar to two-dimensional microscopy images. Weibull showed a poorer fit for carbon fiber composite, while the presence of glass fiber creates a homogenization in porosity variation, also treated by ANOVA. The present methodology enables the prediction of void volume fraction in different carbon/glass preform ratios and stacking sequence along the laminate length and through-thickness. The low glass fiber ratio decreases void content, homogenized porosity distribution along laminate length, and thickness, mainly for glass fiber preforms located in the middle of the laminate. These results confirm that the uniformity of void content throughout the composite can be reduced and controlled by altering the stacking sequence and ratio of glass to carbon fiber preforms. This methodology can be extended to any composite manufacturing process.

Keywords: Hybrid; Laminate/ply; Statistical approach; Void formation.

---

1. Introduction

The presence of a second reinforcement in a polymeric matrix characterizes the most typical type of hybrid fiber-reinforced composite [1], which may be cheap whilst effective from the mechanical behavior point of view given the synergetic behavior of the hybrid system [2–5]. The combination of glass and carbon fibers in a polymeric system can reduce the final material cost due to the high price of carbon fibers [3,6]. Another traditional issue of composite structures is their brittle behavior, which inevitably provides sudden and catastrophic failure with an insufficient warning and low residual load-carrying capacity. In addition, a carbon/glass reinforced polymer hybrid composite can represent a reduction in terms of CO_2 emission, given the less usage of carbon fibers [1,7] since it is originated from fossil fuels [1].

Nonetheless, carbon and glass fibers have distinct microstructures, namely: fiber diameter, architecture, and areal weight of their respective fabrics, which may influence the resin impregnation process during manufacturing the composite [7,8]. The resin flow during composite processing through both reinforcements can directly affect the void content/position/morphology, and hence the final quality of the laminate [9–11], in which the understanding of void formation is vital to understand the mechanical response of the laminate properly.

Porosity (i.e. void) is a detrimental defect that arises from the manufacturing process, and it may play a major role on the mechanical performance of structural composites [12,13]. As an example, porosity may decrease both the static and fatigue strength of the composite [13–15]. Besides, the porosity effect is usually disregarded in the majority of studies, in which the interface is considered perfect and free of voids. In addition to the detrimental impact of void content, void morphology can also have some influence, and this feature is even less exploited than the void content itself. Hamidi et al. [16] demonstrated that the void morphology might have even more influence on the mechanical behavior on composite laminates than the void content, considering that different morphologies could result in distinct stress concentrators. Considering that a fiber-reinforced structural laminate is composed of several plies and that the voids are randomly generated along within the three directions, a proper evaluation of void effects has to take into account the three directions. Thus, a 3D porosity assessment is required, especially regarding its shape, since depending on the 2D angle of observation, the void may have a distinct shape than the real one, which can only be observed three-dimensionally [13,16,17].

Porosity measurement usually shows a high variation across the laminate length and thickness [18,19]. Even using sophisticated techniques for void measurement (e.g., optical microscopy [20], scanning electron microscopy [21], and microscopic computed tomography [17]), its data variation is challenging given the lack of post-processing method to take all effects into account. For reliable analyzes of the measurements, statistical approaches are a feasible way to describe porosity formation since it can reduce the variation according to the reliability level and analyze the variance meaningfully [22,23] instead of merely using deterministic methodologies.

There are no reports dealing with a reliability analysis based on a minimum number of experiments required to enhance the reinforcement content having a homogenized pore characterization (i.e., morphology, location and content), and quantifying the contribution of each fiber on the porosity characteristics. Moreover, elliptical and cylindrical porosity shapes can only be properly identified in 3D images, not addressed so far in the literature. Hence, this technique can be extended to any type of manufacturing process, allowing optimizing the processing parameters for any composite laminate.

Aiming at fulfilling this gap, this work proposes a methodology to unveil the role of voids in carbon/glass fiber-reinforced laminates manufactured via resin transfer molding (RTM) manufacturing process. Porosity content, morphology, and location were measured through 3D optical microscopies and further treated through statistical methods, namely: analysis of variance (ANOVA), normal distribution, and Weibull analysis for variance analysis and reliability determination; and surface response methodology (SRM) for the tendency of void formation.

2. Experimental details

2.1. Materials and processing parameters

Table 1 presents the stacking sequence, fiber volume fraction, and epoxy system of the composites used in this study. Non-hybrid laminates are referred as CFC (carbon fiber reinforced composite) and GFC (glass fiber reinforced composite). Two different hybrid composites are manufactured: H-S1 (interleaving fabric stacking sequence), and H-S2 (glass fiber located in the middle of the laminate). The use of both stacking sequences proposed is to create the maximum number of hybrid interface (i.e., interleaved stacking sequence) and minimum one (glass fiber concentrated in the middle), keeping the symmetry according to the classical lamination theory [24].

Table 1. Details for the hybrid composites herein studied.

Nomenclature	*Fiber volume fraction (%)	Stacking sequence
CFC	53.91	$[(0/90)(90/0)]_{7S}^{C}$
GFC	55.53	$[(0/90)(90/0)]_{7S}^{G}$
H-S1	52.55	$[(0/90)_1^C(90/0)_1^G]_{7S}$
H-S2	52.55	$[(0/90)_{4S}^C(0/90)_{3S}^G]_S$

**Calculated following* [12]*. C – carbon fiber fabric, and G – glass fiber fabric.*

The composites are processed using: PRISM EP2400 epoxy resin (from Cytec, Solvay group); glass fiber non-crimp fabric (0/90), from Barracuda C-0900; and carbon fiber plain weave fabric, from Hexcel AS4-GP. The carbon/glass fiber ratio for hybrid laminates was 50% (v/v). The dimensions of the laminates are 420 × 300 × 3 mm^3. The composites are processed by RTM using a Radius 2100cc injector with an injection pressure of 0.25 MPa at 120 °C. The curing parameters are: 180 °C for 120 min. The processing parameters ensure a capillary number between 0.025 – 0.0025 to generate voids as low as possible [15,25]. The improvement of the capillary setting is performed through permeability tests following Darcy's law, following an earlier study using the same epoxy system (see supplementary material).

The permeability analysis follows the same parameters as the aforementioned epoxy resin. Glycerin and distilled water are used to ensure 100 mPa·s of viscosity. The images of the test (see supplementary material) are used to measure the impregnation behavior.

2.2. Porosity characterization

Porosity measurement is carried out on the cross-sectional area of the specimen, i.e., through-thickness, using an Axio Imager·Z2m optical microscope, with 200× of magnification. Prior to image analyses, the specimens are cut off from the laminate and polished using a sequence of sandpaper from 9 to 1 μm diamond suspension and finished with 0.05-μm alumina suspension. The 2D surface images are then extrapolated to create 3D images.

A typical porosity characterization is depicted in Figure 1, in which Figure 1a exhibits the specimen cross-section; Figure 1b shows the threshold applied to porosity; Figure 1c presents the 2D porosity highlighted; and Figure 1d the 3D porosity measurement. According to the Abbe concept [26] and the applied magnification (objective of Zeiss, epiplan – neofluar 200× with a numerical aperture of 0.9), the theoretical lateral resolution of the studied images is 490 nm.

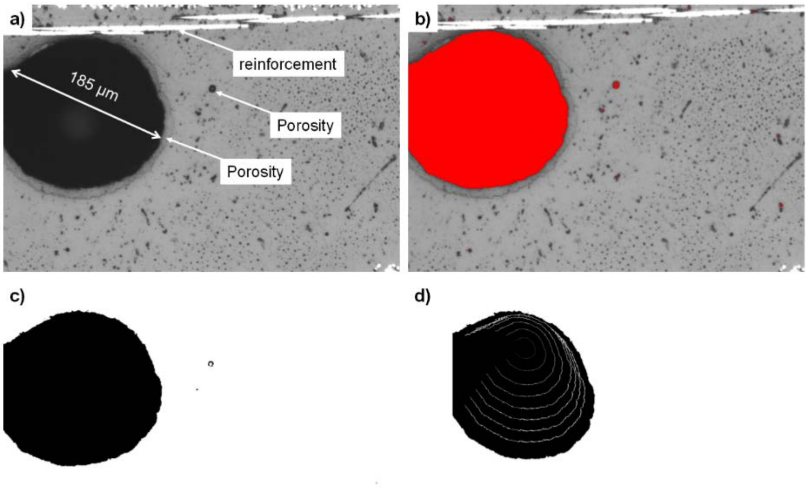

Figure 1. Porosity measurement procedures: a) composite section image, b) porosity with threshold, c) 2D porosity, and d) 3D porosity.

The polishing steps to remove a surface layer of ∼10 μm are used and, following each layer removal, surface images at different layers through-thickness are captured. The control of the polishing step to remove the thin layer is carried out using a digital micrometer. Each specimen dimensions were 3 × 15 × 3 mm^3. Dividing the width in each 10-micron layer removed results in 3,000 images analyzed per specimen. The dimension ensures the same thickness, providing equal analysis between thickness and specimen width. The 2D-images are stacked within 10-micron spacing between each other aiming to ensure greater proximity to 3D reality. By removing both resin and fiber from the images and maintaining only voids, the images remain on their original size ≈0.4 × 0.4 mm^2 (black color for pores and white color for the rest). Therefore, the pores are aligned from the outline of the original image dimension. Besides, different positions are analyzed along the laminate length (10, 200, and 400 mm along the laminate length), in which five specimens for each area were used for the porosity measurement.

2.3. The statistical distribution of void variation

ANOVA method is applied to perform a variance analysis of the porosity results, as well as the quantification of different types of reinforcements on the void formation. The single factor methodology with repetition was used for a comparison of the influence of parameters on the response [22]. A normal distribution is also performed to measure the void content distribution for each laminate. Moreover, a Weibull distribution is applied to reduce the porosity variance in values with reliable levels.

In order to measure the reliability level of the data, a Weibull model (Eqs. (1,2)) is employed; The variable x represents the measurement porosity; β is the shape parameter – whether the distribution tends to exponential ($\beta = 1$) or polynomial ($\beta > 1$); α is the scale parameter – associated to the porosity value scale measured; and $F(x)$ is the density probability that describes the relative probability of the porosity variable taking a given value, directly proportional to the reliability level ($R(x) = 1-F(x)$).

$$F(x) = 1 - exp[-({}^{x}/_{\alpha})]^{\beta} \tag{1}$$

$$\ln\left(\ln\left({}^{1}/_{R(x)}\right)\right) = \beta \cdot \ln(x) + \beta \cdot \ln(\alpha) \tag{2}$$

2.4. *Void content simulation*

For predicting different behaviors of void formation in the hybrid laminates, the response surface methodology (RSM) is applied (Eq. (3)) to describe the interaction among the combination of different void fractions in the hybrid composites and the void formation (morphology and position through-thickness and laminate length). This section aims to reduce the number of experiments required for the porosity prediction in different hybrid laminates, ensuring low cost and experimental time and keeping statistical relevance [22,27]. For a better forecast with small error, the maximum, medium, and minimum levels are selected, as explained in the supplementary material.

$$Y = \beta_0 + \sum_{i=1}^{k} \beta_i x_i + \sum_{i=1}^{k} \beta_{ii} x_i^2 + \sum_{j=1}^{k} \beta_j x_j + \sum_{j=1}^{k} \beta_{jj} x_j^2 + \sum_{i=1}^{k-1} \sum_{j=i}^{k} \beta_{ji} x_i x_j + e \tag{3}$$

where, Y represents the predicted response (i.e., porosity value), x_i and x_j are parameter variations – x_i represents the x-axis (reinforcement type fraction – R_f) and x_j is the y-axis (diameter size – D_s; laminate length – L; thickness – t), β_0 is the constant coefficient; β_i is the linear coefficient; β_{ij} is the interaction coefficient; and e the error.

3. Results and discussion

3.1. *Preform properties*

The impregnation behavior, which is also responsible for void formation, is presented in Table 2. The combination of lower fiber volume fraction with intermediate tortuosity creates lower preform resistance to the flow for hybrid composites, resulting in higher flow velocity and permeability than non-hybrid composites. Carbon fiber preform presents higher resistance to flow compared to glass fiber preform due to their smaller fiber diameter, which allows higher fabric compaction, resulting in larger tortuosity to the flow and greater difficulty to the impregnation flow [7]. Likewise, glass fiber preforms present higher fiber diameter, which makes the reinforcement compaction more difficult, creating larger spaces between adjacent fibers. The areas formed between glass fibers create a natural flow path with less tortuosity way. Thus, the combination of both reinforcements provides a synergetic impregnation behavior. The variation in the impregnation behavior is covered in the next sections through the porosity characterization.

Table 2. Preform impregnation characteristics.

Specimen	Tortuosity	Resistance rate	Flow velocity ($\times 10^{-4}$ m·s^{-1})	Average Permeability ($\times 10^{-10}$ m^2)
CFC	2.22	1.20	3.29	0.62 ± 0.6
GFC	2.08	1.16	13.76	2.57 ± 0.2
H-S1	2.15	1.35	18.07	3.38 ± 0.4
H-S2	2.14	1.12	19.20	3.59 ± 0.2

3.2. Porosity characterization

In this section, the 3D porosity is treated by ANOVA to measure the variance and it shows how the values deviate from the average. The average and deviation values of porosity show the importance of checking if there is a significant difference between the averages and if the reinforcement type influences the void content. Hence, reliable predictions and tendencies of void formation with more realistic values can be obtained, even with high standard deviation. When the standard deviation of porosity results is high, the comparison of effects may not be reliable, therefore, the importance of applying variance analysis as well as determining the reliability of the results.

Figure 2a exhibits porosity values for all samples of this study. CFC presents the highest void content (3.73% ± 0.83), confirming the difficulty to impregnate the entire carbon fiber preform. GFC exhibits the lowest void content (0.94% ± 0.01). As can be clearly seen, the addition of glass fiber into carbon fiber decreases the void content. GFC laminate impregnation ensures a decrease in the void formation and lower standard deviation, indicating a greater homogeneity of pore distribution along the plate with less deviation. Now evaluating the hybrid systems, H-S2 shows void formation lower than H-S1, indicating that when glass performs are positioned in the middle of composite, a lower void formation and higher homogeneity is obtained.

Figure 2b shows the local porosity in each component of the system (i.e., carbon fiber intratow, glass fiber intratow, and intertow). The variance observed in CFC (Fig. 2a) is mostly influenced by the difficulty of impregnation inside the carbon fabric tow, generating higher variation than porosity in the intertow system. GFC exhibits nearly the same porosity between inter and intratow, evidencing a balanced void distribution. In other words, larger spaces between glass fibers facilitate the impregnation flow.

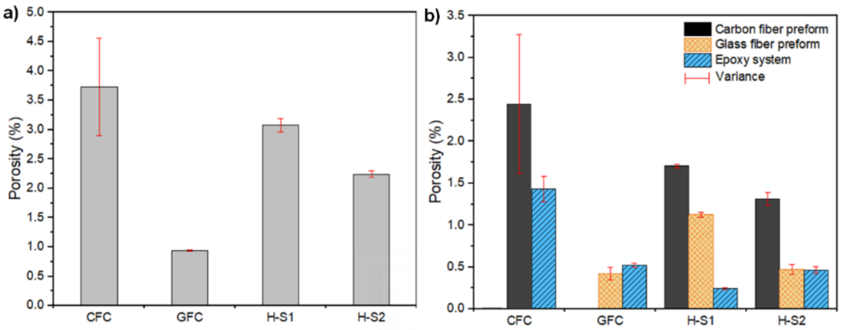

Figure 2. ANOVA of porosity: a) whole composite and b) local porosity at each component of the hybrid system.

The interleaved hybrid stacking sequence (H-S1) shows higher void content in the reinforcement tow than in the intertow, indicating a similar impregnation to the carbon fiber laminate. Even with the addition of glass fiber, H-S1 laminate shows high void content (3.08% ± 0.12); however, H-S1 presents mean value and variance value of 17% and 85%, respectively, lower than CFC, whereas H-S2 shows average and variance value 40% and 92%, respectively, lower than CFC specimen. The concentration of glass fiber in the middle of the laminate (H-S2) decreases the porosity in the composite. H-S2 keeps the same void formation behavior in intertow and glass fiber intratow components as a result shown for GFC, evidencing a balanced void distribution and low variance. H-S2 specimen also keeps similar tendencies observed in non-hybrid laminates with the advantage to have less carbon fiber in its stacking sequence, whereas H-S1 shows intermediate porosity compared to non-hybrid composites, without significant reduction of porosity (compared with H-S2). H-S2 presents a reduction of porosity in terms of average and variance of 27% and 50%, respectively, compared to H-S1.

Figure 3 shows the normal distribution of porosity for each laminate. Figure 3a shows the results for all laminates (further results in supplementary material). The void distribution for CFC has larger normal distribution and lower peak of density, associated with a higher standard deviation of the results. There is a trend in decreasing the opening of the normal curve and increasing the peak frequency to lower pore values following this order: CFC > H-S1 > H-S2 > GFC. This behavior confirms the higher tendency for void formation in CFC, the lower trend for GFC, and intermediate behavior for both hybrid laminates, in which porosity formation in H-S2 is more prone to have lower porosity values with lower deviation, compared to CFC.

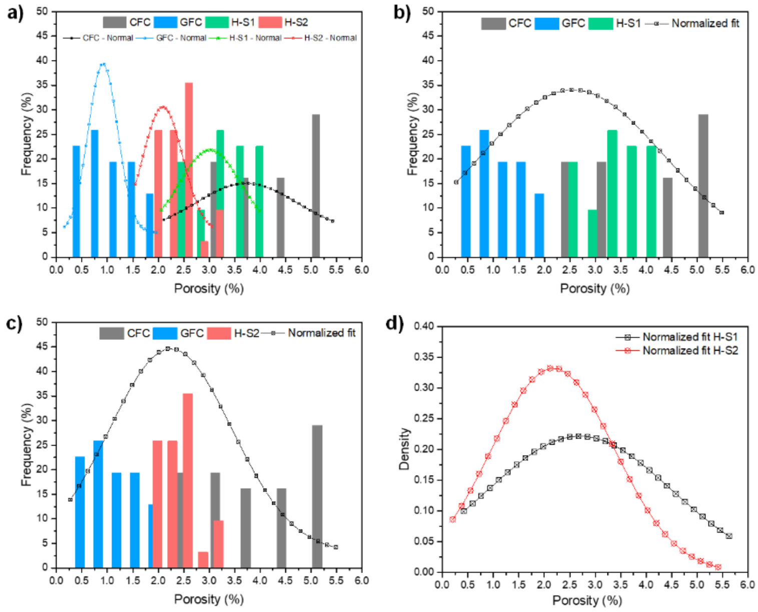

Figure 3. Normal porosity distribution for: a) all laminates, b) non-hybrid comparison with H-S1, c) non-hybrid comparison with H-S2 and d) comparative analysis of normalized fit.

Figures 3(b,c) show the normal distribution tendency in comparison with non-hybrid porosity behavior and H-S1 and H-S2, respectively. This combination shows that glass fiber preforms located in the middle of the laminate decreases the opening of the normal curve, and concentrated higher concentration of porosity in 2% (Figure 3d). The significant variation of the results could result in an inappropriate comparison analysis since some results might be overlapped, as shows Figures 3(b,c), in which hybrid laminates present porosity values similar to CFC and GFC. Therefore, the importance of the analysis of variance between the results evidence which reinforcement type influences the formation of pores by considering their intrinsic standard deviation.

Using ANOVA, it is also possible to measure the percentage of contribution (PC) of each material in the void formation. Porosity tends to be formed mainly in carbon fiber intratow with 53.90% of PC, compared with the intertow (26.20 %) and glass fiber intratow (19.80%). Thus, the addition of glass fiber is a feasible solution to reduce porosity, since the space between reinforcement allows an easier flow path compared to carbon fiber preform.

For a better understanding of the variation of the results, ANOVA is applied with the f-test method aiming at evaluating the variation of results for the same material and different composites. The highest F value indicates the relation with the most influence on the response. For that case, the variance in the results (reinforcement type in Table 3) suggests that the deviation among the families of specimens has more impact than the intrinsic variation for the same material. This is confirmed with a *p-value* lower than 0.05, which keeps the confidence within 95% and the F value higher than $F_{critical}$. Furthermore, PC value confirms that the intrinsic variation only contributes with 4.28% of porosity results; meanwhile, the difference among laminate types shows 86.50% of the contribution. This analysis confirms that void formation is more influenced by reinforcement type, also regarding the high standard deviation of the specimens.

Table 3. ANOVA results.

	F	***p-value***	$\boldsymbol{F_{critical}}$	***PC***
Specimen intrinsic variation	1.39	0.03	5.14	4.28%
Reinforcement type	18.75	0.01	4.75	86.50%

Regarding void deviation, the Weibull method is applied to reduce the variation in reliability level *versus* porosity (Figure 4) [28]. Dashed lines indicate the curve predicted via Weibull analysis, and dots are experimental replications to confirm the procedure. The slope of the curve indicates more variation in porosity as a function of reliability, a result of a greater porosity divergence values (more significant variance). CFC specimen presents a more pronounced curvature, which is due to the significant variance of the results. As a consequence, experimental results show a poorer fit for the CFC Weibull curve. The presence of glass fiber creates a homogenization in porosity variation, showing an appropriate fit between the Weibull model and experimental data. Considering that ANOVA shows how relevant the porosity analysis is between different composites, any value above 20% of reliability confirms that the CFC has more porosity, followed by H-S1, H-S2, and GFC. When considering 90% of reliability, CFC presents 5.12% of void content, GFC = 1.10%, H-S1 = 3.54%, and H-S2 = 2.58%.

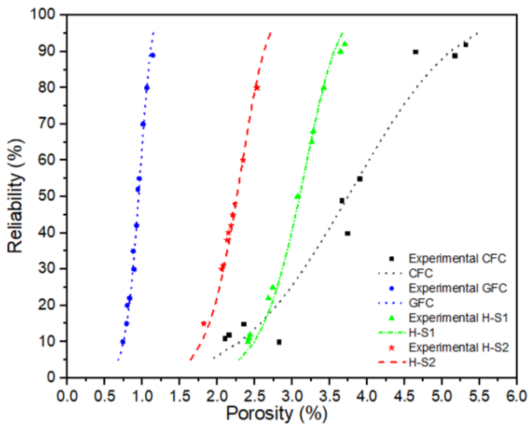

Figure 4. Porosity Weibull distribution versus reliability: CFC; CFV; H-S1; and H-S2.

3.3. *Morphology characterization*

The understanding of morphology of voids is an essential means to characterize the composite properties, considering that void morphology describes void size and shape [16]. The 3D method herein employed ensures proper quantification for measuring morphology. Figure 5 shows 2D and 3D porosity of elliptical and cylindrical shapes. It is difficult to provide the real shape of void in 2D images (Figures 5a,c) since both images have similar formats. Only in 3D images (Figures 5b,d), through sectioned images, it is possible to guarantee their real shapes, either elliptical or cylindrical.

Figure 6 shows the porosity frequency by number (number of times that pores appear with a specific format) and by volume (frequency of total volume). The void format was measured by Eq. (4,5) [29,30], in which circularity is represented by $R = 1$ and elliptical voids with ratios lower than 0.95.

$$D = \sqrt{\frac{4A}{\pi}} \tag{4}$$

$$R = \frac{D}{L_{max}} \tag{5}$$

where, D is void diameter, A is the area, R is dimensionless value for the porosity shape, and L_{max} is the maximal diameter of porosity.

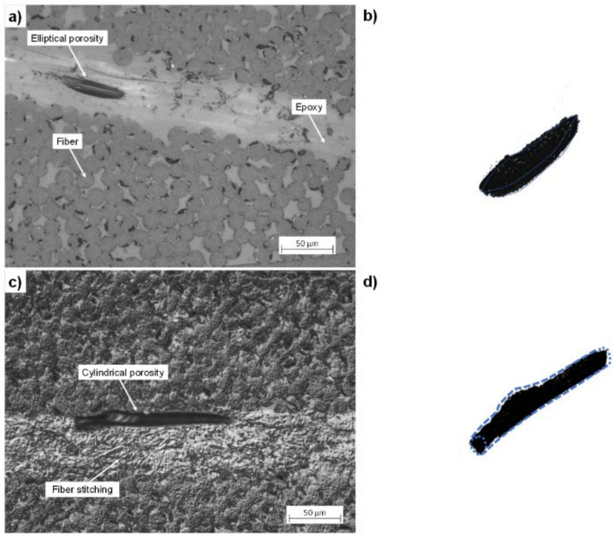

Figure 5. Porosity morphology: a) 2D elliptical, b) 3D elliptical, c) 2D cylindrical and d) 3D cylindrical.

Circular porosity shape has the highest frequency, and the second was elliptical for CFC and H-S1, which indicates that the interleaved hybrid stacking sequence keeps both void content and morphology similar to CFC, as a result of the difficulty to impregnate both preforms. On the other hand, elliptical porosity appearance is more pronounced in GFC and H-S2 specimens, which can be attributed to higher circular void movement resulting from easier flow path (mainly through glass fibers), causing the coalescence of circular voids or the inclination and flattening of porosity due to shear resulted from infusion pressure [15]. Cylindrical voids, mainly found in intra-tow and glass fiber stitching, and irregular porosity show insignificant frequency.

Porosity analysis by the number of appearances or volume is vital because even voids with low frequency in number can occupy larger spaces and cause significant damage, such as premature fatigue fracture, crack initiation and growth, delamination, and decrease of mechanical strength [31,32]. For that purpose, Hamidi et al. [16] established small voids as being lower than 50 μm diameter, medium voids in the range of 50–100 μm, and large pores greater than 100 μm diameter.

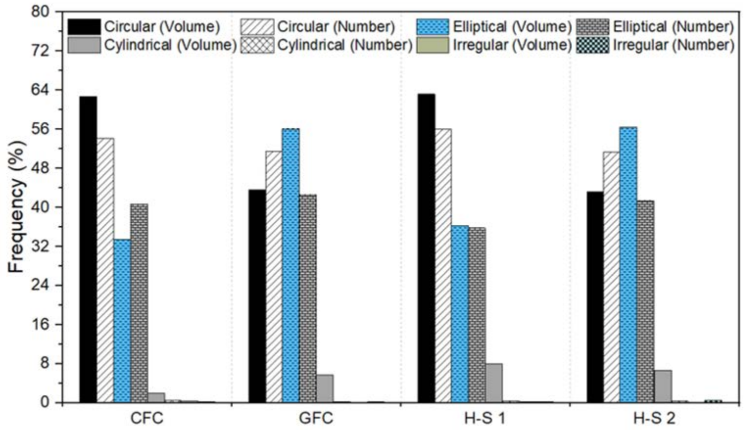

Figure 6. Void shape distribution frequency by number and volume.

Figure 7 exhibits frequency volume and number of diameters (number of diameters with the same size). All laminates present the highest frequency of porosity in the range of 20–40 µm and an insignificant amount of pores higher than 70 µm. Meanwhile, for CFC, the volume frequency shows that medium and larger porosity present higher influence (since they represent the highest volume), and the highest range is displaced to the range of 30-50 µm. A similar behavior occurs with GFC, H-S1, and H-S2, in which medium and larger porosities show higher frequency when the volume is considered. For volume frequency analysis, the highest value is displaced for 50-60 µm (i.e., medium pores) for GFC, H-S1, and H-S2.

Still evaluating Figure 7, CFC reveals a stronger influence of small porosity, considering the difficulty of impregnation in the small spaces among fibers tows. A similar behavior is found for GFC composite. However, the presence of medium and larger porosity increases for GFC due to the higher space between glass fiber and the presence of stitching compared with CFC. This behavior is also reproduced for both hybrids, which indicates that the presence of glass fiber decreases void content and increase medium and larger volume frequency of porosity.

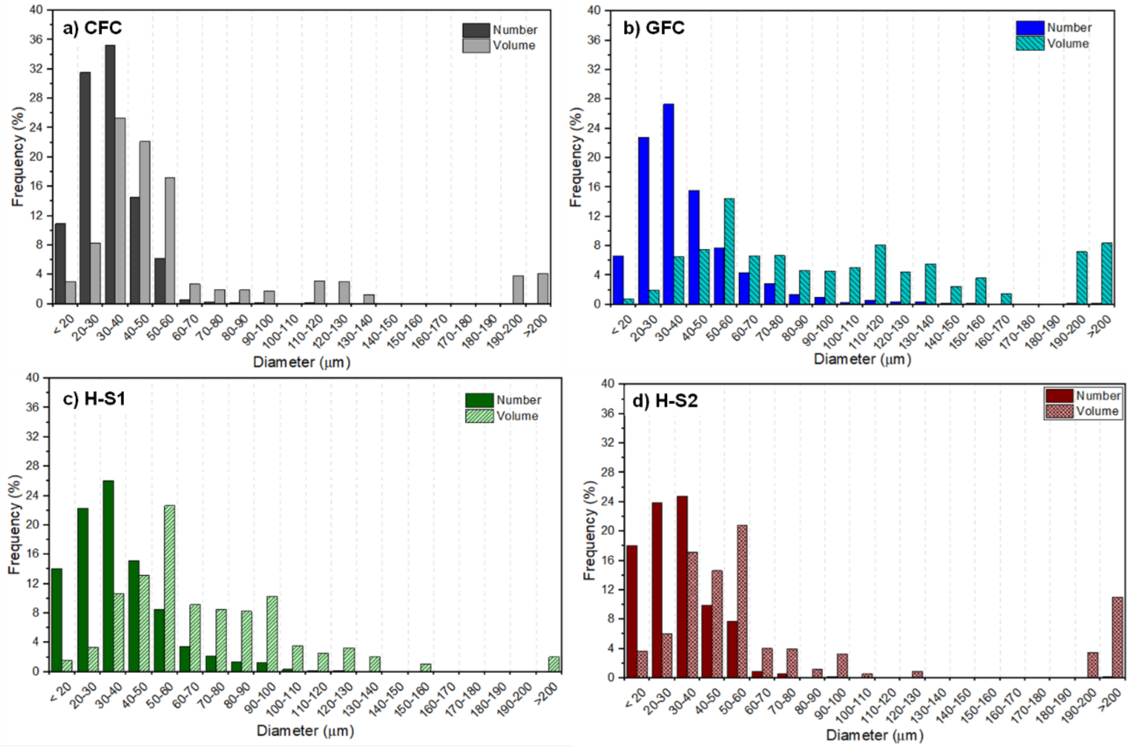

Figure 7. Distribution of void diameters for: a) CFC, b) GFC, c) H-S1, and d) H-S2 samples.

3.4. Void distribution simulation

This section presents void characterization, simulated void content, and morphology for all laminates in study. For this purpose, the SRM (Eq. (3)) is to predict the trend of void formation between explanatory variables, in which the error is described in terms of an equation after each SRM herein presented. As a matter of fact, this method is used to predict void formation and morphology behavior with different reinforcement fractions for an appropriate reinforcement ratio application (carbon/glass), aiming to control porosity characteristics (content, position, and morphology). According to Monticeli et al. [23], the use of higher and lower levels of each parameter is the minimum requirement for SRM application. However, the addition of intermediate levels ensures a smaller error analysis, shown in each SRM equation. In addition, experimental values represented by black dots, evidenced in all SRM graphics, represents the experimental points that control and determine the SRM behavior. The great advantage of this application is the reduction of the experimental number required to void formation prediction in different hybrid laminates ratio [22].

Figure 8 depicts the diameter frequency *versus* carbon/glass fiber ratios. Equations (6-7) show the equations that describe the surface response for Figure 8(a,b), respectively. Both hybrid laminates show a similar relation in diameter distribution, in which the highest frequency is observed in small diameters for CFC. Once glass fiber is added, this distribution becomes more homogeneous for the other diameter frequency (including medium and larger ranges). This analysis shows an error lower than 5%.

In the view of laminate length, Figure 9 presents the variation of carbon/glass fiber ratio on the void content along the laminate length. Equations (8-9) show the formulas to reproduce Figure 9(a,b) results. CFC presents the lowest permeability and highest porosity variation, which means that it is more difficult to impregnate the entire laminate, due to the higher resistance to the flow path. GFC presents a linear impregnation and low void content along the whole composite, which indicates that the addition of glass fiber into carbon fiber reduces porosity deviation and content.

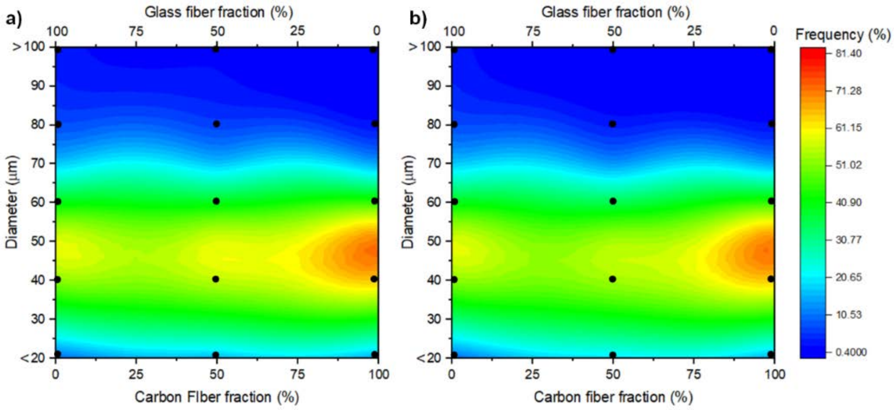

Figure 8. SRM diameter frequency versus carbon fiber (bottom axis) and glass fiber (upper axis) ratio variation: a) interleaved stacking sequence and b) glass fiber concentrated in the middle.

$$V_C\ (mm) = 19.1 - 16.9R_f + 0.8D_s - 34.1R_f^2 + 0.2D_s^2 - 3.5R_fD_s + 0.0343 \quad (6)$$

$$V_C\ (mm) = 18.6 - 17.5R_f + 0.8D_s - 31.1R_f^2 + 1.9D_s^2 - 3.5R_fD_s + 0.0467 \quad (7)$$

Figure 9a shows the interleaved void formation along the laminate length. Only laminates with the glass ratio content of 50% result in homogenized pore distribution along the laminate length. For values greater than 50% of carbon fiber content, it maintains a high resistance and increases the pore fraction, mainly at the laminate edges. Likewise, the concentration of glass fiber in the middle of the composite (Figure 9b) decreases porosity formation. Using a ratio of 75% carbon fiber and 25% of glass fiber tends to result in the same behavior compared to the 50/50 carbon/glass composite. For the second stacking sequence (H-S2 - Figure 9b), lower addition of glass fiber is required for an exponential decrease of porosity, as well as a more homogeneous distribution throughout the laminate length with low glass fiber ratio content.

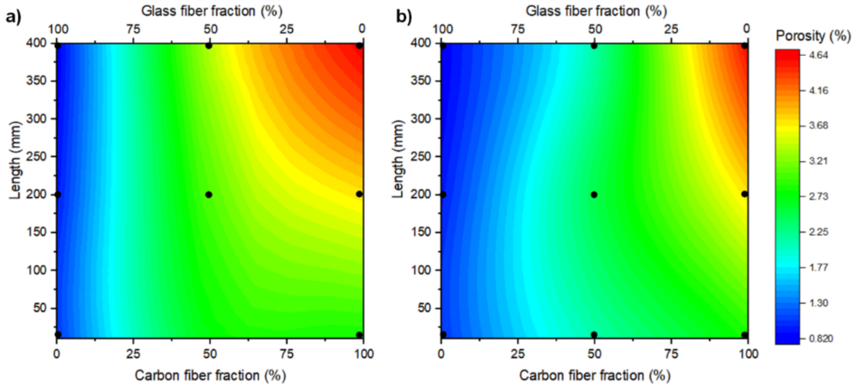

Figure 9. SRM laminate length versus carbon fiber (bottom axis) and glass fiber (upper axis) ratio variation: a) interleaved stacking sequence and b) glass fiber concentrated in the middle.

$$V_C\ (\%) = 2.6 + 0.4R_f + 1.4L + 0.01R_f^2 - 0.7L^2 + 0.5R_fL + 0.0886 \quad (8)$$

$$V_C\ (\%) = 2.3 + 0.3R_f + 1.4L - 0.1R_f^2 + 0.09L^2 + 0.5R_fL + 0.0621 \quad (9)$$

Figure 10 presents the variation in porosity varying the carbon/glass fiber ratio through-thickness. Equations (10-11) show the equations that describe the SRM plot shown in Figure 10(a,b), respectively. Interleaved hybrid laminate (Figure 10a) has a constant variation of void through-thickness, attributed to the impregnation properties of each fabric. This variability in void formation is related to an uneven impregnation flow, which is a result of the similarity void formation with CFC. Besides, the second stacking sequence (H-S2 – Figure 10b) also shows a variation through-thickness (according to each fabric proportion and position). However, the presence of glass fiber in the middle keeps a low fraction of porosity (in the middle) and decreases void formation in carbon preform, in which a considerable reduction of porosity is observed from 25% of glass fiber addition, and also reduces pores in the carbon fiber (positioned in upper and bottom surfaces). The results show an error lower than 10%, evidenced in each equation. The error is lower for void simulation regarding morphology analysis since this analysis shows lower variation for each reinforcement type.

Such behavior is reported in the study performed by Calado et al. [33], in which during a linear impregnation flow though fabrics with different characteristics (Figure 11a), a secondary flow in the thickness direction is reported. This new direction of impregnation guarantees a better wetting of the reinforcement with worse permeability (Figure 11b). This results in less pore formation across the plate (length and thickness). As a matter of fact, H-S2 sample ensures better porosity control to laminate length and thickness, and this behavior tends to be kept with less glass fiber ratio content.

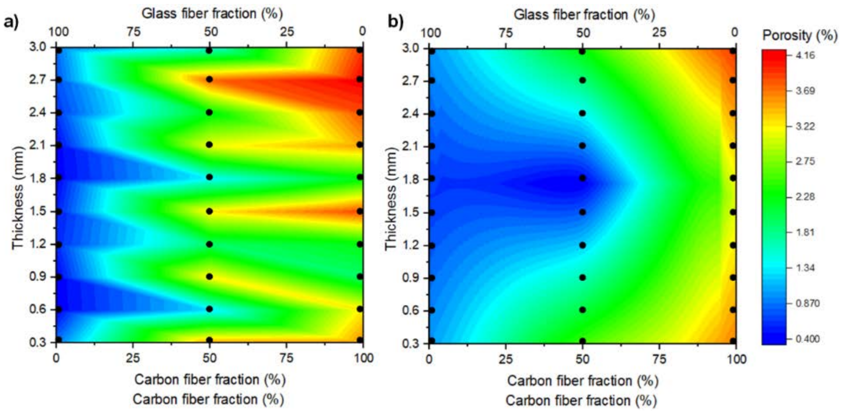

Figure 10. SRM laminate thickness *versus* carbon fiber (bottom axis) and glass fiber (upper axis) ratios: a) interleaved stacking sequence and b) glass fiber concentrated in the middle.

$$V_C\ (\%) = 2.1 - 0.3R_f + 1.7t + 0.9R_f^2 - 0.8t^2 + 0.4R_f t + 0.0873 \quad (10)$$

$$V_C\ (\%) = 1.8 - 0.3R_f + 1.7t + 3.5R_f^2 + 0.3t^2 + 0.8R_f t + 0.0518 \quad (11)$$

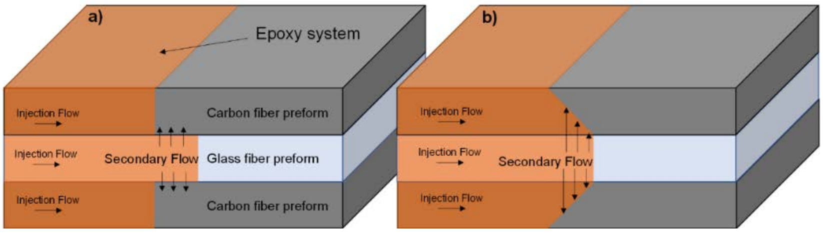

Figure 11. Second thickness flow direction with two reinforcement: a) initial impregnation and b) second flow behavior.

4. Conclusions

In this study, the importance of void characterization via statistical approaches through a 3D methodology is developed, which allows distinguishing void morphology, which is not possible by a 2D approach. The void content, location, and morphology are analyzed by a profound statistical approach, including Weibull, normal distribution, and ANOVA approaches. Permeability tests have shown that carbon fiber has more tortuosity compared to glass fibers, which hinders flow impregnation. The inclusion of glass fibers at different positions in the hybrid composite changes permeability and, consequently, reflecting directly on void size, shape, and distribution. The high level of void deviation generated the need to apply statistical tools, which confirms and quantifies that the reinforcement used influences the void formation.

Normal distribution and ANOVA methods treat the void variance, and the main results show a balanced void distribution for glass fiber composite, i.e., larger spaces among glass fibers in comparison to carbon fibers facilitate resin impregnation. It is a feasible solution to reduce void content. Weibull method confirms that void deviation is higher for carbon fiber composite due to a higher variation of the results. Furthermore, the interleaved composite follows the carbon fiber composite regarding porosity shape (circular), and higher porosity diameter and shape (elliptical or cylindrical) are predominant for glass fiber and the hybrid with glass fiber in the middle, mainly found in intra-tow and fiber stitching. Concluding, the addition of glass fiber decreases void content and increase porosity shape size for hybrid laminates.

The simulation tendency confirms that low ratio of glass fiber fabric decreases void content, homogenized porosity distribution along laminate length and thickness, due to a second thickness flow, mainly for the second hybrid stacking sequence (H-S2 – glass fiber preforms located in the middle of the laminate). The simulation performed is a feasible method to determine the appropriated carbon/glass fiber preform ratio and stacking sequence to determine void content aiming the balance of material cost and laminate impregnation quality.

Acknowledgments

The authors acknowledge the epoxy resin donation from Solvay group; and the financial support from FAPESP (process number: 2015/19967-4 and 2017/10606-4) and CAPES.

References

[1] Swolfs Y, Gorbatikh L, Verpoest I. Fibre hybridisation in polymer composites: A review. Compos Part A Appl Sci Manuf 2014;67:181–200. https://doi.org/10.1016/j.compositesa.2014.08.027.

[2] Monte Vidal DC da S, Ornaghi HL, Ornaghi FG, Monticeli FM, Voorwald HJC, Cioffi MOH. Effect of different stacking sequences on hybrid carbon/glass/epoxy composites laminate: Thermal, dynamic mechanical and long-term behavior. J Compos Mater 2020;54:731–43. https://doi.org/10.1177/0021998319868512.

[3] Guermazi N, Haddar N, Elleuch K, Ayedi HF. Investigations on the fabrication and the characterization of glass/epoxy, carbon/epoxy and hybrid composites used in the reinforcement and the repair of aeronautic structures. Mater Des 2014;56:714–24. https://doi.org/10.1016/j.matdes.2013.11.043.

[4] Almeida Jr. JHS, Amico SC, Botelho EC, Amado FDR. Hybridization effect on the mechanical properties of curaua/glass fiber composites. Compos Part B Eng 2013;55. https://doi.org/10.1016/j.compositesb.2013.07.014.

[5] Da Silva LV, Júnior JHSA, Angrizani CC, Amico SC. Short beam strength of curaua,

sisal, glass and hybrid composites. J Reinf Plast Compos 2013;32. https://doi.org/10.1177/0731684412467561.

[6] Czél G, Jalalvand M, Wisnom MR. Demonstration of pseudo-ductility in unidirectional hybrid composites made of discontinuous carbon/epoxy and continuous glass/epoxy plies. Compos Part A Appl Sci Manuf 2015;72:75–84. https://doi.org/10.1016/J.COMPOSITESA.2015.01.019.

[7] Monticeli FM, da Silva Monte Vidal DC, Shiino MY, Voorwald HJC, Cioffi MOH. Hybrid-permeability model evaluation through concepts of tortuosity and resistance rate: Properties of manufactured hybrid laminate. Polym Eng Sci 2019;59:1215–22. https://doi.org/10.1002/pen.25104.

[8] Salvatori D, Caglar B, Teixidó H, Michaud V. Permeability and capillary effects in a channel-wise non-crimp fabric. Compos Part A Appl Sci Manuf 2018;108:41–52.

[9] Ali MA, Umer R, Khan KA, Cantwell WJ. In-plane virtual permeability characterization of 3D woven fabrics using a hybrid experimental and numerical approach. Compos Sci Technol 2019;173:99–109. https://doi.org/10.1016/j.compscitech.2019.01.030.

[10] Kuentzer N, Simacek P, Advani SG, Walsh S. Correlation of void distribution to VARTM manufacturing techniques. Compos Part A Appl Sci Manuf 2007;38:802–13. https://doi.org/10.1016/j.compositesa.2006.08.005.

[11] Yun M, Carella T, Simacek P, Advani S. Stochastic modeling of through the thickness permeability variation in a fabric and its effect on void formation during Vacuum Assisted Resin Transfer Molding. Compos Sci Technol 2017;149:100–7. https://doi.org/10.1016/j.compscitech.2017.06.016.

[12] Monticeli FM, Daou D, Dinulovic M, Jacobus H, Voorwald C, Hila MO. Mechanical behavior simulation : NCF / epoxy composite processed by RTM. Polym Polym Compos 2019;27:66–75. https://doi.org/10.1177/0967391118817174.

[13] Mehdikhani M, Gorbatikh L, Verpoest I, Lomov S V. Voids in fiber-reinforced polymer composites: A review on their formation, characteristics, and effects on mechanical performance. J Compos Mater 2019;53:1579–669. https://doi.org/10.1177/0021998318772152.

[14] de Almeida SFM, Neto ZDSN. Effect of void content on the strength of composite laminates. Compos Struct 1994;28:139–48. https://doi.org/10.1016/0263-8223(94)90044-2.

[15] Monticeli FM, Ornaghi HL, Cornelis Voorwald HJ, Cioffi MOH. Three-dimensional porosity characterization in carbon/glass fiber epoxy hybrid composites. Compos Part A Appl Sci Manuf 2019;125:105555. https://doi.org/10.1016/j.compositesa.2019.105555.

[16] Hamidi YK, Aktas L, Altan MC. Three-dimensional features of void morphology in resin transfer molded composites. Compos Sci Technol 2005;65:1306–20.

https://doi.org/10.1016/j.compscitech.2005.01.001.

[17] Papapetrou VS, Patel C, Tamijani AY. Stiffness-based optimization framework for the topology and fiber paths of continuous fiber composites. Compos Part B Eng 2020. https://doi.org/10.1016/j.compositesb.2019.107681.

[18] Lam RC, Kardos JL. The permeability and compressibility of aligned and cross-plied carbon fiber beds during processing of composites. Polym Eng Sci 1991;31:1064–70. https://doi.org/10.1002/pen.760311411.

[19] Demaría C, Ruiz E, Trochu F. In-Plane Anisotropic Permeability Characterization of Deformed Woven Fabrics by Unidirectional Injection. Part II: Prediction Model and Numerical Simulations. Polym Compos 2007;28:812–27. https://doi.org/10.1002/pc.

[20] Bodaghi M, Cristóvão C, Gomes R, Correia NC. Experimental characterization of voids in high fibre volume fraction composites processed by high injection pressure RTM. Compos Part A 2016;82:88–99.

[21] Elomaa L, Kokkari A, Närhi T, Seppälä J V. Porous 3D modeled scaffolds of bioactive glass and photocrosslinkable poly(ε-caprolactone) by stereolithography. Compos Sci Technol 2013;74:99–106. https://doi.org/10.1016/j.compscitech.2012.10.014.

[22] Monticeli FM, Montoro SR, Voorwald HJC, Cioffi MOH. Porosity Characterization of Carbon Fiber / Epoxy Composite Using Hg Porosimetry and Other Techniques. Polym Eng Sci 2020;1:1–9. https://doi.org/10.1002/pen.25343.

[23] Monticeli FM, Ornaghi HL, Neves RM, Odila Hilário Cioffi M. Creep/recovery and stress-relaxation tests applied in a standardized carbon fiber/epoxy composite: Design of experiment approach. J Strain Anal Eng Des 2019:1–9. https://doi.org/10.1177/0309324719892710.

[24] Daniel IM, Ishai O. Engineering mechanics of composite materials. 2nd ed. New York: Oxford University Press; 2006.

[25] Hamidi YK, Aktas L, Altan MC. Three-dimensional features of void morphology in resin transfer molded composites. Compos Sci Technol 2005;65:1306–20. https://doi.org/10.1016/j.compscitech.2005.01.001.

[26] Hell SW, Dyba M, Jakobs S. Concepts for nanoscale resolution in fluorescence microscopy. Curr Opin Neurobiol 2004;14:599–609. https://doi.org/10.1016/j.conb.2004.08.015.

[27] Debnath S, Reddy MM, Yi QS. Influence of cutting fluid conditions and cutting parameters on surface roughness and tool wear in turning process using Taguchi method. Measurement 2016;78:111–9. https://doi.org/10.1016/j.measurement.2015.09.011.

[28] Gao X, Dodds RH, Tregoning RL, Joyce JA, Link RE. A Weibull stress model to predict cleavage fracture in plates containing surface cracks. Fatigue Fract Eng Mater Struct 1999;22:481–93. https://doi.org/10.1046/j.1460-2695.1999.00202.x.

[29] Hamidi YK, Aktas L, Altan MC. Effect of packing on void morphology in resin transfer molded E-glass/ epoxy composites. Polym Compos 2005;26:614–27. https://doi.org/10.1002/pc.20132.

[30] Zdilla M, Hatfield S, McLean K, Cyrus L, Laslo J, Lambert H. Circularity, solidity, axes of a best fit ellipse, aspect ratio, and roundness of the foramen ovale: a morphometric analysis with neurosurgical considerations. J Craniofac Surg 2017;27:222–8. https://doi.org/10.1097/SCS.0000000000002285.Circularity.

[31] Zhang Y, Zhang L, Yin X, Liu Y, He Z, Zhang J. Effects of porosity on in-plane and interlaminar shear strengths of two-dimensional carbon fi ber reinforced silicon carbide composites. Mater Des 2016;98:120–7. https://doi.org/10.1016/j.matdes.2016.03.017.

[32] Li Y, Li Q, Ma H. The voids formation mechanisms and their effects on the mechanical properties of flax fiber reinforced epoxy composites. Compos PART A 2015;72:40–8. https://doi.org/10.1016/j.compositesa.2015.01.029.

[33] Calado VMA, Advani SG. Effective average permeability of multi-layer preforms in resin transfer molding. Compos Sci Technol 1996;56:519–31.